

An Optimized Robotic Scanning Scheme for Ultrasonic NDT of Complex Structures

Z. Xiao¹  · C. Xu¹ · D. Xiao¹ · F. Liu¹ · M. Yin¹

Received: 19 September 2016 / Accepted: 4 April 2017 / Published online: 23 May 2017
© The Society for Experimental Mechanics, Inc 2017

Abstract To reduce the inspection time for evaluating defects in geometrically complex structures, this study investigates a more efficient scheme in which the test object is grasped by the robot (TOGR). Compared with the traditional approach in which the ultrasonic probe is grasped by the robot (UPGR), the TOGR solution consumes less time in the inspection of complex specimens because fewer joints are involved in the scanning motion. A six-degrees-of-freedom industrial robot is used to hold the non-destructive testing (NDT) probe normal to the test surface, and ultrasonic time-domain reflectometry (UTDR) is used to identify the flaw echo. The ultrasonic signals are acquired synchronously with positional data regarding the robot. The TOGR solution shows a significant improvement in the positional accuracy of the robotic trajectory. The distribution of defects inferred via ultrasonic C-scan imaging is plausible, as verified by the stable surface echo in the time domain during an experimental test. The TOGR solution is well suited for the high-speed automatic inspection of complex structures, such as turbine blades, milling tools and other test specimens with curved surfaces. Experiments were conducted in which NDT data were acquired at scanning speeds of up to 50 mm/s with a minimum defect resolution of 0.15 mm.

Keywords Trajectory planning · Signal acquisition · Ultrasonic C-scan image · Curved surface

✉ Z. Xiao
shawzhen86@gmail.com

¹ School of Mechanical Engineering, Beijing Institute of Technology, Beijing 100081, China

Introduction

Using the traditional manual ultrasonic test (UT) approach to inspect micro-defects in specimens with complex surface shapes is difficult because of the challenges associated with manipulating the probe. Robotic scanning technology has received increasing attention because of its greater repeatability and accuracy. Moreover, robot arms can help to access areas and inspect geometries for which manual inspection is not practical.

Several methods for establishing automated inspections of complex parts have been proposed and implemented in recent decades. Bogue Robert described the development of robotic applications in the field of ultrasonic non-destructive testing (NDT) [1]. Mineo Carmelo et al. [2] proposed a synchronous acquisition system for robotic trajectory and NDT data based on the phased array UT technique. Sattar T.P. et al. designed a portable NDT robotic arm that can be carried by climbing and walking robots; this arm is equipped with a force sensor that is used to scan complex shapes by keeping the NDT probe normal to the surface to maintain a constant contact force [3]. Compared with manual inspection, robotic scanning technology has enabled significant improvements in the quality of inspection results [4].

Modern industrial robots can manipulate probes faster and more accurately than is possible in other NDT inspection methods. However, the robotic trajectory should be optimized to reduce the inspection time, and factors that influence the efficiency of the robotic scanning motion, some of which are rarely considered in the existing approaches, should be investigated. In applications of industrial robots in NDT, the specimen is typically fixed, and the ultrasonic probe is grasped by the robot (UPGR) [5]. In this case, the scope of motion of the robotic arm is affected by the layout of the gripper and the water circulation equipment [6]. In particular, if the specimen

needs to be rotated during the inspection, some auxiliary components, such as a swivel table, are needed. Moreover, revolving the robot around the test object is difficult because of the singular point [6]. This paper presents a new approach in which the test object is grasped by the robot (TOGR). A new algorithm based on coordinate transformation is proposed for planning the robot's path. Whereas other solutions require several joint motions and rotations, the proposed TOGR solution sometimes requires only one joint rotation for the inspection of axisymmetric specimens. Compared with the UPGR solution, the proposed TOGR method is more efficient and suitable for high-speed inspection.

The geometry of the test object must be known to generate the robotic trajectory. The geometric model of the test object is usually known a priori or is measured through reverse engineering methods [7]. A computer-aided drawing (CAD) representation of the part should be used. The part position relative to the robot reference system must be accurately calibrated for precise robotic path execution and to keep the ultrasonic probe normal to the test surface. The ultrasonic energy generated by the ultrasonic transducer will penetrate the specimen surface more efficiently if the relative position between the test object and the probe is accurately controlled, which will maximize the damage/defect detection sensitivity [8, 9].

Another important requirement for reliable ultrasonic inspection is to maintain a constant distance between the probe and the test surface, along with a constant ultrasonic incidence angle. Maintaining this distance is relatively easy for simple geometries, such as flat samples, rotational parts or other symmetric specimens, which can be inspected automatically using traditional NDT approaches. However, complex shapes require more advanced scanning solutions for proper inspection at high speeds. Because of trajectory errors, contact detection methods are inappropriate for specimens with complex geometries. Therefore, the longitudinal wave method is used to detect the internal defects of such a test object; the incidence angle is subject to fewer constraints when this non-contact method is used because the robotic trajectory can be adjusted to accommodate the errors to a certain extent [10, 11].

In general, the trajectory planning algorithm should guarantee the positional accuracy of the robot. Tavakoli Mahmoud et al. [12] described several schemes for controlling the probe orientation during the inspection of industrial pipelines. Sattar Tariq, et al. [3] designed a climbing robot for inspecting aircraft wings and fuselages; the sensor was carried by a mobile robot, and the positional data were simulated in MATLAB. Kalra Love P et al. [13] proposed a surface coverage algorithm for a climbing robot that autonomously scans the wall surface and performs the necessary inspection tasks; the orientation of the robot is compensated according to feedback from the NDT sensors. Mineo Carmelo et al. [14] described software that enables accurate robot tool paths to be executed through an innovative external control approach. This method overcomes

the limitations of traditional off-line programming approaches when applied to NDT measurements. However, these software algorithms were designed for the case of a fixed specimen, with the probe being manipulated by the robot.

This paper describes the advantages of the new TOGR inspection approach which is suitable for the fast, automated inspection of small complex parts; this method is particularly efficient when the primary necessary motion is the rotation of the part around one axis (for symmetric specimens). Reversing the traditional UPGR approach can significantly reduce the necessary movement range. The mathematical model represents the coordinate conversion between the reference coordinate system of the robot and the work-piece coordinate system. The robot positions are calculated using a CAD model of the specimen. In this study, an ultrasonic inspection is performed by collecting the ultrasonic energy that is reflected by the back wall of the specimen or by flaws within the specimen. The collected data are then analyzed to find the flaws. The experimental results verify the accuracy and validity of the proposed robotic path-planning algorithm. This method allows a more accurate robotic trajectory for inspecting turbine blades, which produces better ultrasonic data and, therefore, a better non-destructive evaluation (NDE) through ultrasonic C-scan imaging. Ultrasonic C-scans consist of ultrasonic signals encoded through the robot feedback positions.

Trajectory Planning of the Robot

Although industrial robots are commonly used in various fields of industrial on-line testing, the positional accuracy of the robotic trajectory should be improved for NDT applications. Generating an accurate robot tool path for the ultrasonic inspection of complex geometries is challenging, and the TOGR approach requires the development of new algorithms. For the traditional situation in which the probe is manipulated by the robot, a CAD model of the part is the necessary input. In this case, the tool path is usually generated using off-line path planning software based on computer-aided manufacturing (CAM) algorithms. The TOGR approach requires additional computations to transform the positions and orientations of the robot into the work-piece coordinate system.

In this paper, a turbine blade is inspected by the industrial robot STAUBLI TX90L, which has 6 degrees of freedom (DOFs) and whose end effector is designed to be sealed and waterproof. Both the TOGR and UPGR solutions are implemented to determine the more efficient solution and the minimum motion of the robot arm. In the UPGR approach, all trajectory points for the ultrasonic scan of the target specimen are generated using CAM software. The kinematic parameters

required by the robot manipulator are obtained by considering the requirements for ultrasonic NDT scanning.

Process of Trajectory Planning

The robotic trajectory for the TOGR approach is generated by applying a newly developed coordinate conversion algorithm to the discrete points that are generated by the CAM software for the traditional UPGR method. This algorithm consists of the following steps:

- 1) The coordinates of the UPGR trajectory points are transformed into the work-piece coordinate system (as shown in Fig. 1(a)).
- 2) Robotic simulations are generated by the CAM post-processor. The robotic scanning motion can be treated as the trajectory of a milling tool, and the kinematic parameters can be adjusted as needed.
- 3) The coordinates and normal vector of each point are exported to be post-processed by a MATLAB script. Transforms consisting of the rotational matrix for each point of the trajectory are generated.
- 4) The trajectory command positions are sent to the robot controller.
- 5) The command positions are adjusted to maximize the amplitude of the ultrasonic energy. This final task is driven by the experimental results.

Manufacturing Simulation

Figure 2 shows a turbine blade tool path, which consists of numerous green points that cover the entire surface. The distance between two adjacent points can be adjusted to satisfy

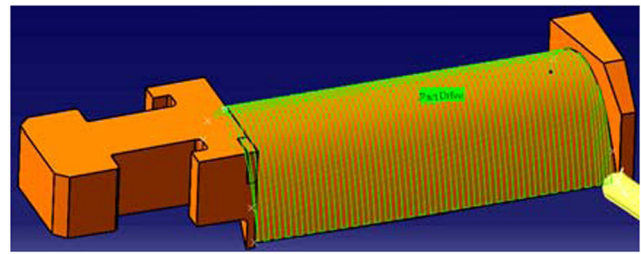


Fig. 2 Tool path for a turbine blade

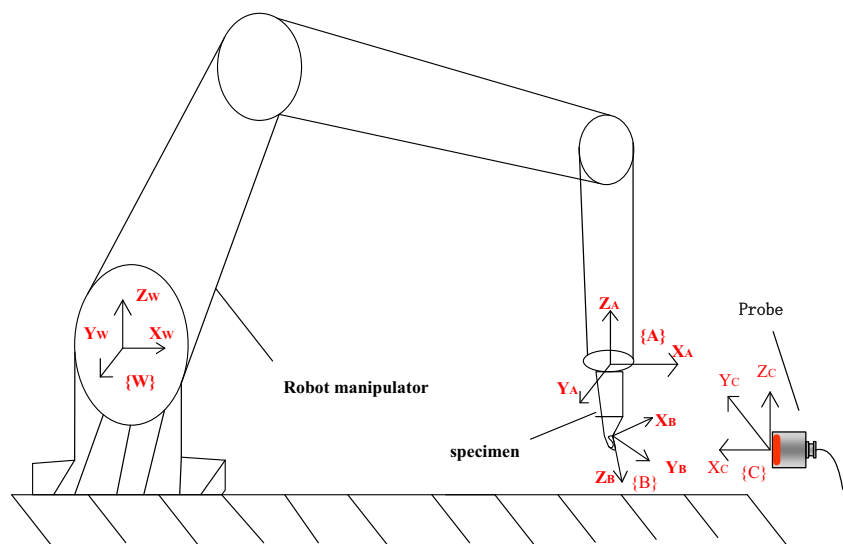
the NDT requirements, including the sampling interval and line spacing.

Matrix Transformation

Four coordinate frames are defined for the robotic system, as shown in Fig. 1: the work-piece coordinate system $\{A\}$, the auxiliary coordinate system at each discrete point $\{B\}$, the reference coordinate system of the robot $\{W\}$ (called the world coordinate frame) and the user frame $\{C\}$ (in this paper, this is defined as the coordinate system of the probe) [15]. In the UPGR approach, the position and orientation of the robot in the work-piece coordinate system are obtained. This information is generated by the CAM post-processor and is arranged in a row array of the form $[x, y, z, \psi_x, \psi_y, \psi_z]$, where the first three parameters indicate the location of the discrete point and the last three parameters are the components of the unit normal vector along the x , y and z axes. Then, a rotational matrix based on the array can be constructed to estimate the position and orientation of the robot. Additionally, because a constant ultrasonic incidence angle is guaranteed by the path-planning algorithm, the normal vector is coincident with the beam axis of the probe during automatic inspection.

The TOGR approach requires the rotational matrix that is based on the equivalent matrix relative to the tool frame or to

Fig. 1 The coordinate systems of the robot. *A* Work-piece coordinate system *B* Auxiliary coordinate system *C* Coordinate system of the probe *W* World coordinate frame



the world coordinate frame. Therefore, a new algorithm should be developed to generate an accurate robotic trajectory so that the robotic end effector can be controlled as planned.

An industrial robot with 6 DOFs, known as STAUBLI TX90L, is used for ultrasonic NDT inspection in this paper. The rotation sequence of this robot obeys the X-Y-Z Euler angle-set convention [13]. Supposing that there is a vector labeled ${}^A P$ in $\{A\}$, the orientations of the same vector in $\{B\}$ and $\{C\}$ can be labeled as ${}^B P$ and ${}^C P$, respectively. Then, the transform matrix denoted by ${}^A C T$ describes the orientation of the robotic end effector after the transformation from ${}^A P$ to ${}^C P$.

According to coordinate conversion theory, ${}^A C T$ is equal to the matrix product ${}^A B T {}^B C T$, and the transform matrices ${}^A B T$ and ${}^B C T$ can be solved based on the geometry of the original discrete points.

$${}^A P = {}^A B T {}^B C T {}^C P = {}^A C T {}^C P \tag{1}$$

Since there is no singular point on the milling-tool path, the transform between $\{A\}$ and $\{C\}$ is reversible. Therefore, ${}^A C T$ can be decomposed into a rotation matrix, denoted by ${}^A R$ and a translation matrix, denoted by ${}^C P_{AORG}$.

$$\begin{aligned} {}^A C T &= \begin{bmatrix} {}^A R & {}^C P_{AORG} \\ 0 & 1 \end{bmatrix} = \begin{bmatrix} {}^C R^T {}^B R^T & {}^C R^B P_{AORG} + {}^C P_{BORG} \\ 0 & 0 & 0 & 1 \end{bmatrix} \\ &= \begin{bmatrix} {}^C R^T {}^B R^T & -{}^C R^B P_{BORG} + {}^C P_{BORG} \\ 0 & 0 & 0 & 1 \end{bmatrix} \end{aligned} \tag{2}$$

$${}^A R = {}^A P^B P^{-1} = \begin{bmatrix} \xi_X & \varphi_X & \psi_X \\ \xi_Y & \varphi_Y & \psi_Y \\ \xi_Z & \varphi_Z & \psi_Z \end{bmatrix} \tag{3}$$

$\xi = [\xi_X, \xi_Y, \xi_Z]^T$ — the representation of the x components in $\{A\}$ relative to $\{B\}$;

$\varphi = [\varphi_X, \varphi_Y, \varphi_Z]^T$ — the representation of the y components in $\{A\}$ relative to $\{B\}$; and

$\psi = [\psi_X, \psi_Y, \psi_Z]^T$ — the representation of the z components in $\{A\}$ relative to $\{B\}$;

$${}^B C R = {}^B P^C P^{-1} \tag{4}$$

If the orientation of $\{B\}$ coincides with that of $\{C\}$, then ${}^B C R$ is a unit matrix; if the normal vectors of $\{B\}$ and $\{C\}$ are opposite, then ${}^B C R$ is the following diagonal matrix:

$${}^B C R = \begin{bmatrix} 1 & 0 & 0 \\ 0 & -1 & 0 \\ 0 & 0 & -1 \end{bmatrix} \tag{5}$$

Thus, ${}^A C T$ can be simplified into the following matrix:

$${}^A C T = \begin{bmatrix} {}^B R & -{}^B R^T {}^A P_{BORG} \\ 0 & 0 & 0 & 1 \end{bmatrix} \tag{6}$$

When the robotic end effector moves to a given discrete point as planned, the origin points of the auxiliary coordinate frame and the user frame overlap. Moreover, a constant ultrasonic incidence angle is guaranteed if the spatial relationship between $\{B\}$ and $\{C\}$ is correctly considered.

A definite transform matrix is calculated following the rotation sequence rule, known as the X-Y-Z Euler convention.

$$\begin{aligned} R_{X-Y-Z} &= R_X(\alpha)R_Y(\beta)R_Z(\gamma) \\ &= \begin{bmatrix} 1 & 0 & 0 \\ 0 & \cos\alpha & -\sin\alpha \\ 0 & \sin\alpha & \cos\alpha \end{bmatrix} \begin{bmatrix} \cos\beta & 0 & \sin\beta \\ 0 & 1 & 0 \\ -\sin\beta & 0 & \cos\beta \end{bmatrix} \begin{bmatrix} \cos\gamma & -\sin\gamma & 0 \\ \sin\gamma & \cos\gamma & 0 \\ 0 & 0 & 1 \end{bmatrix} \\ &= \begin{bmatrix} c\beta c\gamma & -c\beta s\gamma & s\beta \\ s\alpha s\beta c\gamma + c\alpha s\gamma & -s\alpha s\beta s\gamma + c\alpha c\gamma & -s\alpha c\beta \\ -c\alpha s\beta c\gamma + s\alpha s\gamma & c\alpha s\beta s\gamma + s\alpha c\gamma & c\alpha c\beta \end{bmatrix} \end{aligned} \tag{7}$$

In matrix (7), α , β , and γ are the Euler angles that indicate the values of the changes between the beginning and ending orientations of the robotic end effector; parameters such as $\cos\alpha$ and $\sin\alpha$ are abbreviated to $c\alpha$ and $s\alpha$ for clarity.

Six parameters should be delivered to the robot controller, including the position coordinates of the discrete point relative to the world coordinate frame of the robot and the Euler angles $[\alpha, \beta, \gamma]$. By substituting the solution for matrix (7) into ${}^A R$, which is a component of matrix (6), ${}^A C T$ can be solved when ${}^A P_{BORG}$ is obtained from the geometry of the test object.

The Euler angles for each discrete point can be calculated as follows:

$$\begin{aligned} \beta &= \text{atan2}\left(\psi_x, \sqrt{\xi_x^2 + \varphi_x^2}\right) \\ \alpha &= \text{atan2}\left(-\psi_y / \cos\beta, \psi_z / \cos\beta\right) \\ \gamma &= \text{atan2}\left(-\varphi_x / \cos\beta, \xi_x / \cos\beta\right) \\ {}^{BB} P_{AORG} &= -{}^A R^T [x, y, z] \end{aligned} \tag{8}$$

Therefore, the parameters $[{}^B P_{AORG}, \alpha, \beta, \gamma]$ can be calculated and delivered to the robot controller. However, certain parameters such as the Denavit-Hartenberg parameters and the Euler angles are necessary for a new robot; the positional matrices of discrete points can be derived from these input parameters [16].



Transformation of the Robotic Trajectory

The robotic trajectory can be expressed as a point cloud that is obtained from the tool path of a numerical control (NC) machining simulation (as shown in Fig. 3).

The locations of the discrete points, labeled as $[X, Y, Z]$ relative to the world coordinate frame, are read from the controller in real time. Then, the corresponding points on the test surface, labeled as $[X_0, Y_0, Z_0]$ relative to the work-piece coordinate system, can be computed by solving the inverse kinematic problem:

$$\begin{bmatrix} X \\ Y \\ Z \end{bmatrix} = -R_{X'-Y'-Z'} \begin{bmatrix} X_0 \\ Y_0 \\ Z_0 \end{bmatrix} \quad (9)$$

By substituting equation (7) into the transform matrix $R_{X'-Y'-Z'}$, the real-time locations of the discrete points can be calculated as follows:

$$\begin{bmatrix} X_0 \\ Y_0 \\ Z_0 \end{bmatrix} = -R_{X'Y'Z'}^{-1} \begin{bmatrix} X \\ Y \\ Z \end{bmatrix} \quad (10)$$

The mathematical models of the coordinate conversions between the reference coordinate system of the robot and the work-piece coordinate system are represented simultaneously, and the orientation of the robotic end effector can be controlled using the proposed coordinate conversion algorithm.

Simulation of the Robotic Trajectory

The TOGR solution is simulated in the pre-processor of the manipulator, as shown in Fig. 4. The primary motion of the robot is small-scale rotation, which is less time-consuming for the TOGR solution than for the UPGR solution at the same velocity.

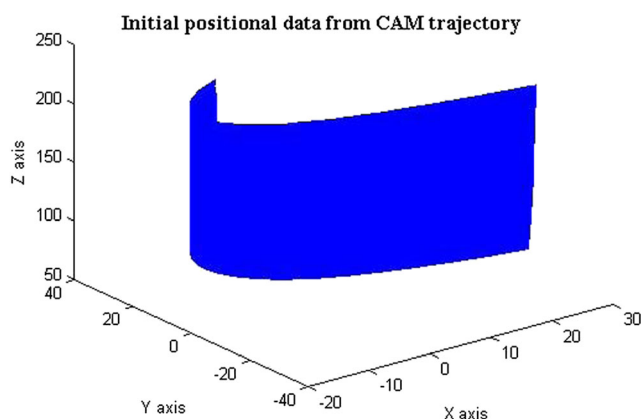


Fig. 3 Point cloud of a simulated tool path

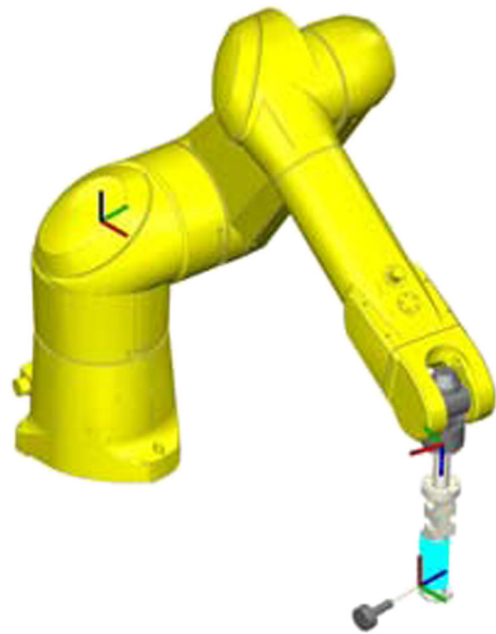


Fig. 4 Simulation of the robotic path with the TOGR solution

Ultrasonic Signal Acquisition and Processing

A UT system was constructed based on the TOGR solution; Fig. 5 shows the design prototype. The system includes the probe, A/D acquisition card, signal generator, industrial robot, and computer.

Experimental Design and Components

Several tests were performed using the TOGR and UPGR solutions. With the planned robotic trajectory guaranteeing the correct orientation, the test object is maintained at a constant distance from the probe. Performance parameters of the apparatus are listed in Table 1.

In this system, a straight Olympus immersion focusing probe is fixed on the platform, a voltage of 400 V is applied to excite the longitudinal wave probe with a 10 kHz pulse repetition frequency, and the UTDR method is used to collect the ultrasonic echo waves. Considering energy attenuation,

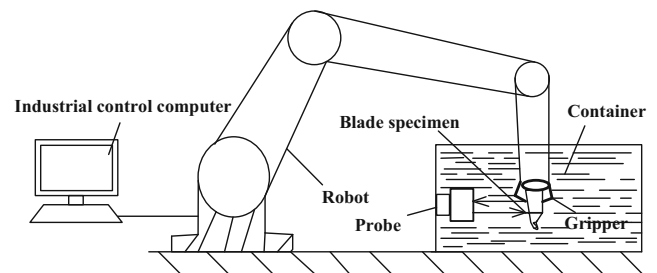


Fig. 5 The prototype NDT system

Table 1 Components of the UT system

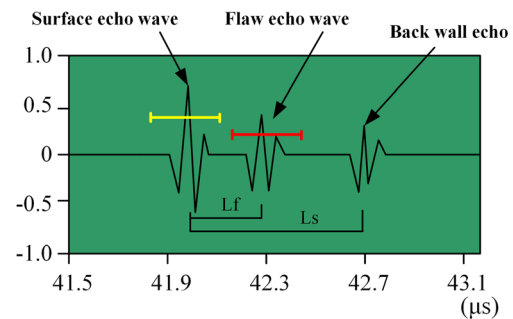
Apparatus	Model & Characteristics	
	Brand	Property
Robot	STAUBLI TX90L	6DOFs, 250 mm/s(max)
Ultrasonic probe	Olympus	10 MHz, immersion focusing
A/D acquisition card	Acquisition Logic AL12200	12bit, sample rate:200 MHz
Signal generator	Olympus PR5077	Repetition frequency:10 kHz
Gripper	Non-standard	Connect the specimen to the robot end effector
Container	Non-standard	Volume: 500 L

the ultrasound incidence angle should be constant, and the echo waves will be reflected along the beam axis, as planned by the orientation constraint of the robotic trajectory. The location of the robot and the corresponding ultrasonic signal are collected synchronously to constitute the test results; the positional data are provided by the controller, and the ultrasonic signal is collected by the A/D acquisition card. Since all data are collected sequentially, the flaw characteristics can be correctly distinguished from the ultrasonic A-scan waves. Furthermore, the integrity of the specimen can be examined using ultrasonic C-scan imaging, which presents the distribution of flaws inside the specimen.

Signal Acquisition and Processing

Synchronous acquisition of the discrete point locations and the ultrasonic signal is crucial to the UT system, since the threads that collect the ultrasonic reflected wave echoes and the real-time robotic positional data are independent. During an NDT experiment, the echo reflected from the flaws, located between the surface echo wave and the back-wall echo wave, can be distinguished from the A-scan waves [17].

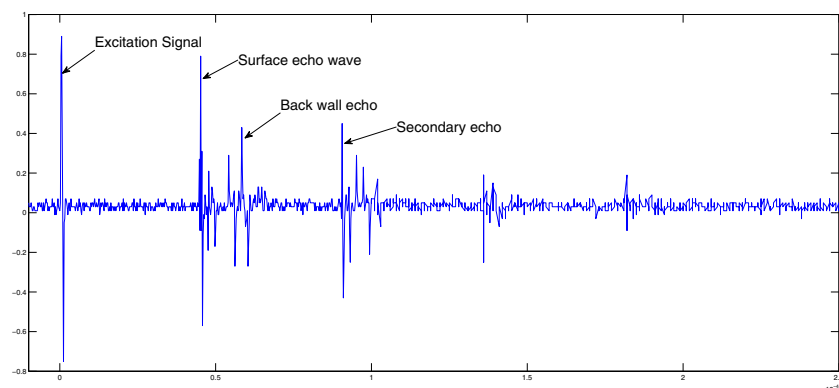
Figure 6 shows the reflected ultrasonic echo waves in the time domain; only the region between the surface echo wave and the back-wall echo wave is investigated. The signal that

**Fig. 7** The following gate in the ultrasonic wave

represents the manifestation of a flaw feature is explored based on the peak-to-peak value of the flaw echo. As shown in Fig. 7, a following gate (in red) is used to track the region of interest, and several parameters describing the ultrasonic A-scan waves are defined. Thus, a scattered wave in the region of interest cannot influence the acquisition of the feature signals, although refracted waves and diffracted waves are common in the reflected echo waves.

During an automatic inspection, each discrete point of the robotic trajectory corresponds to an ultrasonic echo wave. Real-time observation of the waveforms is necessary for evaluating the specimen's integrity. The delay of the back-wall echo, which is labeled L_s in Fig. 7, changes as the thickness of the specimen varies. The flaw echo is tracked using a threshold gate (shown in red in the figure); if the amplitude of the flaw echo exceeds this threshold, then the peak-to-peak value is recorded as a gray value to form a bright color region. Thus, the distribution of flaws in the specimen can be visualized through ultrasonic C-scan imaging. By contrast, the surface echo is tracked using the threshold gate shown in yellow in the figure; the distance between the flaw and the surface can then be estimated from the parameter L_f , which specifies the region of interest.

To visualize the distribution of flaws in the specimen, waveforms of ultrasonic echoes are collected at different points using the pulse reflection method; Fig. 8 shows several examples. Then, the feature signals of the echo waves can be

**Fig. 6** Ultrasonic waves in the time domain

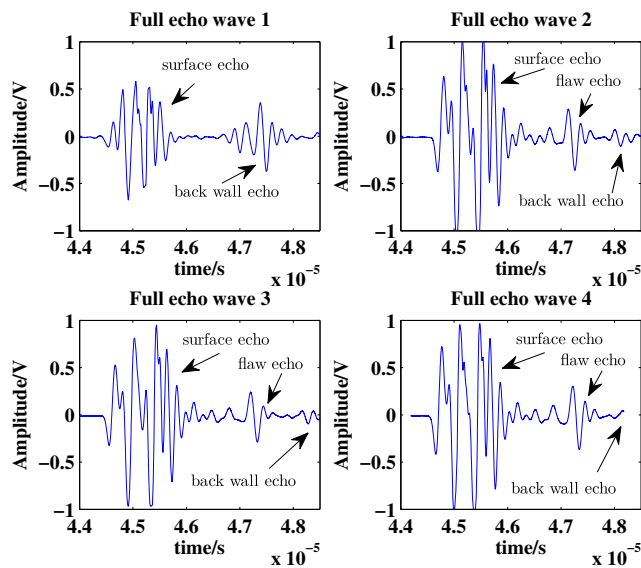


Fig. 8 Ultrasonic waves at different points

analyzed to find the flaws. As shown in Fig. 8, the position of the surface echo is stable and is centered at $45 \mu\text{s}$ in the time domain; therefore, the distance between the probe and the test surface is constant. In addition, the amplitude of the surface echo wave approaches the initial excited value, which indicates that the incidence angle satisfies the requirements. If the amplitude of the reflected surface echo wave decreases, as in the case of full echo wave 1, this indicates that the probe is not normal to the test surface; in this case, the robotic trajectory should be adjusted to more accurately obtain a point with limited energy attenuation.

Although the echoes reflected by specimens of different materials and geometries are diverse, flaw echoes should be distinguishable because of their specific location in the time domain, which is assigned by the inspector prior to the experiment. Furthermore, the amplitude of a flaw echo, which is affected by the geometry and gain bandwidth, will be markedly smaller than that of the surface echo wave because of energy attenuation; therefore, it is necessary to track the flaw echoes in real time using a following gate.

Pixels are assigned gray values that are extracted from the feature signals, and different colors in the region of interest for the specimen are used to identify flaws. There is a one-to-one correlation between the positional data and the pixels where the feature signals are depicted. If the robotic end effector moves 0.15 mm , the real-time positional data provided by the manipulator controller will be updated based on instructions written in the variable assembly language (VAL). Simultaneously, an ultrasonic wave is acquired by the A/D acquisition card when the ultrasonic pulse is excited.

By virtue of this synchronous acquisition, the pixels in the generated ultrasonic C-scan image have the same precision as the repeatable positioning accuracy of the robot, which is 0.08 mm , as declared by the manufacturer. Therefore, the test

results are precise, and the error is within the permissible range.

Experimental Results and Discussion

During practical testing, ultrasonic waves are excited and transmitted through water, which acts as the transmission medium. Then, the waves are reflected when they encounter discontinuities in the specimen. The echo waves are received by the probe and the A/D acquisition card, and the ultrasonic A-scan waves are collected to analyze the feature signals, which represent the flaws characteristics.

Practical Trajectory of the Robot

Since the precision of the robotic trajectory is crucial for the NDE of the specimen, it is necessary to record the real-time position of the robot and to verify the accuracy of the robotic trajectory that is calculated using the proposed algorithm. The positional precision of the robotic trajectory can be estimated based on the distance between the probe and the test surface that is deduced from the ultrasonic A-scan waves in the time-domain.

More than 98,475 discrete points were delivered to the manipulator in the test reported here. The positions along the robotic trajectory were exported from the CAM post-processor and transformed from the initial data into the required equivalent data. To verify the correctness of the planned trajectory, the real-time positional data relative to the reference coordinate system of the robot could be calculated based on the changes in the values of the encoder pulses, output from the manipulator controller every 4 milliseconds.

To improve the positional accuracy of the robotic trajectory, high-density point data that are adapted to match the high-frequency ultrasonic waves are necessary for a specimen with a curved surface. Therefore, an iterative approach, such as the Lagrange multiplier method, is used to generate an interpolation [18].

As illustrated in Fig. 9, if the robotic end effector has the correct orientation, then the normal vector of the auxiliary coordinate system at each discrete point is guaranteed to coincide with the beam axis of the probe; consequently, the energy attenuation of the ultrasonic wave is reduced, as seen from the fact that the amplitude of the surface echo waveform approaches the initial excited value. Otherwise, if the beam axis of the probe is not perpendicular to the test surface, the energy attenuation may be higher. Furthermore, the distance between the probe and the test surface should remain constant, which manifested as a stable position of the surface echo wave in the time domain.

Considering the capacity of the robotic system for the synchronous acquisition of NDT data, the robot velocity was set

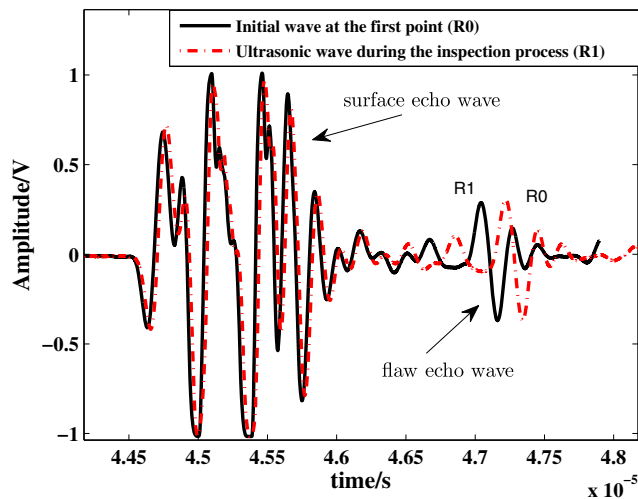


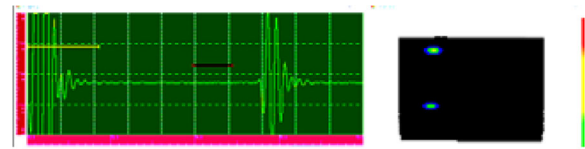
Fig. 9 Repeatability of the robotic trajectory

to 50 mm/s, which, in combination with the 25 MHz sampling rate, is suitable for finding flaws with a minimum equivalent diameter of 0.5 mm; the other scanning conditions were the same between the experiments conducted using both the TOGR and UPGR solutions. Inspecting the turbine blade using the proposed TOGR solution required less than 15 min at this speed of 50 mm/s; at the same velocity, the inspection using the UPGR solution required 22 min, demonstrating that the TOGR solution decrease the inspection time by approximately one third. The required space in which to perform the NDT application using the TOGR solution is also smaller; only rotations of the terminal joint and small-scale up and down movements of the robotic wrist are necessary in this case for inspecting the test object, rather than large-scale motions of several joints or the entire robot.

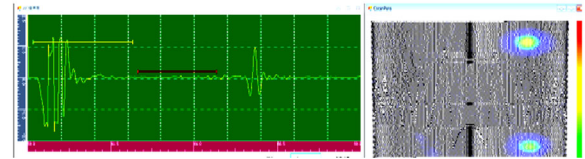
Even when inspecting extremely asymmetric test objects using the TOGR solution, the only possible primary motion is the rotation of the robotic end effector. Fewer joints are involved in this motion, and the detection efficiency is improved. Moreover, the scanning velocity can be more easily increased because the maximum rotational speed of the terminal joint is greater than the maximum movement speed. Therefore, using the TOGR solution can reduce the inspection time for specimens with curved surfaces.

Experimental Results

An integrated system designed for industrial applications was constructed based on the NDT prototype, including the STAUBLI TX90L robot, a conventional ultrasonic longitudinal testing probe, and a signal generator. Several turbine blades with artificial defects were inspected to verify the proposed TOGR solution.



(a) Experimental results obtained using the TOGR solution

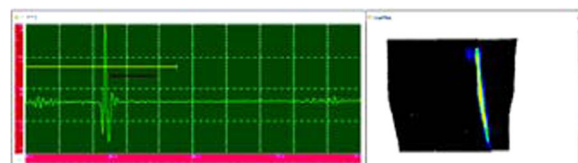


(b) Experimental results obtained using the UPGR solution

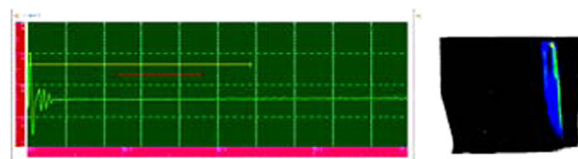
Fig. 10 Ultrasonic C-scan imaging of a specimen with artificial defects as shown in the control software

The ultrasonic A-scan signals were monitored in real time, and the distance L_f was adjusted by modifying the threshold gate used to track the region of interest in the time domain. A turbine blade made of nickel alloy was used in this test, and two flat-bottom holes with diameters of 1.5 mm and 1 mm and depths of 1.5 mm and 1 mm, respectively, were manufactured in the blade. The experimental results obtained using the TOGR solution at a speed of 50 mm/s are shown in Fig. 10(a), and the results obtained using the UPGR solution at the same velocity are shown in Fig. 10(b).

Both the TOGR and UPGR solutions are able to distinguish the two flat-bottom holes, although their automatic inspection accuracy and efficiency differ. The UPGR solution shows image distortion; the pixels shown in white are not assigned positional data because they correspond to times when the speed of the robot exceeded the capability of the system to synchronously record these data and the corresponding feature signal. In particular, several discrete points collected during high-speeds inspection are assigned a null gray value. By contrast, the TOGR solution shows higher



(a) Experimental results obtained using the TOGR solution



(b) Experimental results obtained using the UPGR solution

Fig. 11 Experimental results for a real turbine blade as shown in the control software

efficiency and satisfies the high-speed inspection requirements because each pixel is assigned a gray value that correctly represents the corresponding flaw echo feature signal.

Another test was performed to inspect a turbine blade that had been used in practical applications, with the results shown in Fig. 11. Both the TOGR and UPGR solutions are able to reveal the crack in the blade. The dimensions of the flaw are $5 \times 0.2 \times 0.5$ mm, and the flaw detection precision is approximately 0.15 mm, as calculated from the distance between adjacent points relative to the work-piece coordinate system.

In contrast to the inspection results obtained using the TOGR solution, the UPGR solution visualizes the flaw with some image distortion in the ultrasonic C-scan imaging results. When the robotic scanning velocity exceeds the capability of the UT system, the feature signal within the range of the threshold gate in the A-scan waves is incorrect.

Factors such as the sampling rate and ultrasonic intensity should be considered when they affect the resolution of the C-scan imaging. Experiments were performed to compare the image resolutions achieved using different sampling rates to find an optimal parameter, as shown in Table 2. For the detection of internal defects, one flat sample with four flat-bottom holes with diameters of 0.5 mm, 1 mm, 1.5 mm, and 2 mm, and depths of 1 mm was used, and the minimum sampling rate was explored based on the test results.

Each pixel in the ultrasonic C-scan imaging results has a gray value that is transformed from the peak-to-peak value of the flaw echo wave. If the number of discrete points is not equal to the number of ultrasonic echo waves, then one or more pixels may be assigned a null value; thus, the image resolution is affected by these colorless pixels, especially at smaller total numbers of pixels.

The sampling rate needs to be optimized to detect micro-defects. Several scattered colorless pixels can be observed if

the sampling rate is too low to determine the difference between the feature signals of adjacent points. Therefore, the density of the discrete points should be increased such that the pixels in the display area will be assigned the correct flaw echo signals. According to the test results listed in Table 2, when the sampling rate exceeds 5 MHz, a hole of 1.0 mm in diameter can be identified (verified at 10 MHz); similarly, the sampling rate should exceed 10 MHz when the hole diameter is 0.5 mm (verified at 25 MHz). Thus, the smaller the holes are, the higher the sampling rate should be.

Conclusion and Future Work

In this research, a comprehensive study of a UT system based on the TOGR scanning scheme was conducted to improve the automatic inspection efficiency for complex structures at high speeds. First, an algorithm based on a matrix transform was designed to guide the robotic trajectory planning; then, a mathematical model for the coordinate conversion between the reference coordinate system of the robot and the work-piece coordinate system was developed, to obtain the robot orientations for complex structures. Second, a mechanism for synchronous data acquisition of the positional data of the discrete points, read from the robot controller in real time, and the corresponding ultrasonic flaw echo signals was described. This mechanism is crucial for ultrasonic C-scan imaging to visualize the distribution of flaws in a specimen. Third, the experimental results were shown to be sufficiently precise when all data are collected in real time and the sampling rate is sufficiently high that micro-flaws in the specimen can be conveniently distinguished. Compared with traditional UPGR inspection methods, the proposed method has a higher image resolution, and the influence of the sampling rate has been

Table 2 Optimal sampling rate

Test No.	Sampling rate	Minimum flaw diameter	Number of discrete points	Some pixels with null gray value
1	5 MHz	2 mm	24,158	False
2	5 MHz	1.5 mm	33,681	False
3	5 MHz	1.0 mm	36,052	True
4	5 MHz	0.5 mm	45,278	True
5	10 MHz	2 mm	34,849	False
6	10 MHz	1.5 mm	39,784	False
7	10 MHz	1.0 mm	57,134	False
8	10 MHz	0.5 mm	80,503	True
9	25 MHz	2 mm	55,517	False
10	25 MHz	1.5 mm	98,475	False
11	25 MHz	1.0 mm	131,572	False
12	25 MHz	0.5 mm	157,318	False

examined. Based on the experimental results, the minimum flaw resolution that can be achieved in ultrasonic C-scan imaging is 0.15 mm. Finally, the TOGR scheme has been shown to be promising for industrial applications.

However, only specimens of an appropriate scale can be inspected using the TOGR solution and the ultrasonic transmission method may not be applicable for extremely asymmetric specimens. The attenuation of wave energy is difficult to measure when obtaining an accurate trajectory estimate is challenging due to the ultrasound transmission path, which is determined by the material and geometry. Nevertheless, the automatic inspection precision of a UT system based on ultrasonic technology, such as an ultrasonic phased array or an ultrasonic microscope, can be improved by adopting the TOGR solution. In the future, we plan to inspect small-scale structures using this advanced approach with an acceptable robotic scanning speed. The proposed algorithms can be widely used in large-batch industrial productions.

Acknowledgements This research was funded by the Advanced NC Machine Tools & Basic Manufacturing Equipment, project of the Ministry of Science & Technology of China (Grant No. 2014ZX04012015) and by the National Natural Science Foundation of China (Grant No. 51335001).

References

1. Robert B (2010) The role of robotics in non-destructive testing. *Ind Robot-An Int J* 37(5):421–426
2. Carmelo M, Gareth PS, Ben W, Pascual IN, Ian C (2015) PAUT inspection of complex-shaped composite materials through six DOFs robotic manipulators. *Insight-Non-Destructive Testing and Condition Monitoring* 57(3):161–166
3. Sattar Tariq P, Alina-Alexandra B (2009) Robotic system for inspection of test objects with unknown geometry using NDT methods. *Ind Robot –An Int J* 36(4):340–343
4. Luk BL, Liu KP, Jiang ZD (2009) Robotic impact-acoustics system for tile-wall bonding integrity inspection. *Mechatronics* 19(8): 1251–1260
5. Pedersen MR, Nalpantidis L, Andersen RS, Schou C, Bogh S, Kruger V, Madsen O (2016) Robot skills for manufacturing: from concept to industrial deployment. *Robot Comput Integr Manuf* 37(3):282–291
6. Debanik R (2015) Development of novel magnetic grippers for use in unstructured robotic workspace. *Robot Comput Integr Manuf* 35: 16–41
7. Rowshandel H, Nicholson GL, Davis CL (2011) A robotic approach for NDT of RCF cracks in rails using an ACFM sensor. *Insight* 53(7):368–372
8. Yanzi M, Yang L, Hongbin M, Huijie J (2016) The pose estimation of mobile robot based on improved point cloud registration. *Int J Adv Robot Syst* 13(52):342–350
9. Olivieri P, Birglen L, Maldague X, Mantegh I (2014) Coverage path planning for eddy current inspection on complex aeronautical parts. *Robot Comput Integr Manuf* 30(3):305–314
10. Yongguo Z, Xiang H, Wei F, Shuanggao L (2010) Trajectory planning algorithm based on quaternion for 6-DOF aircraft wing automatic position and pose adjustment method. *Chin J Aeronaut* 23: 707–714
11. Yousif H, Wilcox PD, Todd MD, Drinkwater BW (2014) A probabilistic approach for the optimization of ultrasonic array inspection techniques. *NDT & E Int* 68:43–52
12. Mahmoud T, Lino M, de Almeida AT (2010) Development of an industrial pipeline inspection robot. *Ind Robot - An Int J* 37(3):309–322
13. Kalra Love P, Jason G (2007) An autonomous self Contained Wall climbing robot for non-destructive inspection of above-ground storage tanks. *Ind Robot – An Int J* 34(2):122–127
14. Carmelo M, Pierce SG, Pascual IN, Cooper I (2016) Robotic path planning for non-destructive testing – a custom MATLAB toolbox approach. *Robot Comput Integr Manuf* 37:1–12
15. Paul RP (1981) *Robot manipulators: mathematics, programming, and control*. The MIT Press, Cambridge, Massachusetts and London, England
16. Das A, Waslander SL (2014) Scan registration using segmented region growing NDT. *Int J Robot Res* 33(13):1645–1663
17. Gordon D, Rahul S, Gareth PS (2011) A noncontact ultrasonic platform for structural inspection. *IEEE Sensors J* 11(10): 2458–2468
18. Salmani RA, Reza KH, Saeed H (2015) Adaptive fault detection and isolation for a class of robot manipulators with time-varying perturbation. *J Mech Sci Technol* 29(11):4901–4911